Low-emissivity fine-tuning of efficient VO_2-based thermochromic stacks with silver nanowire networks

Supplementary Materials

Amaury Baret[1], Ambreen Khan[2,3], Aline Rougier[3], Daniel Bellet[3], and Ngoc Duy Nguyen[1]

1) Figure of Merit

As detailed in the main manuscript, our objective is to formulate a FOM of the form $\Delta T_{sol} \times T_{lum}^{n}$, wherein $n > 1$ allows to prioritize higher values of luminous transmittance. In order to determine this ideal n, we compute the FOM associated to a simple stack of VO_2 on glass across varying VO_2 thicknesses. The outcomes, depicted in Fig. S1 for $n = 4$, reveal that in both the thin film and nanoparticles cases, the FOM shape reflects the desirable criteria for practical design integration, *i.e.* T_{lum} exceeding 75% with simultaneous ΔT_{sol} above 15%.

Furthermore, it should also be noted that using $n < 4$ tends to shift the maximum of the FOM curve towards higher VO_2 thicknesses, signifying a requirement for higher ΔT_{sol} than those previously deemed optimal, albeit at the expense of reduced T_{lum} at the maximum FOM values.

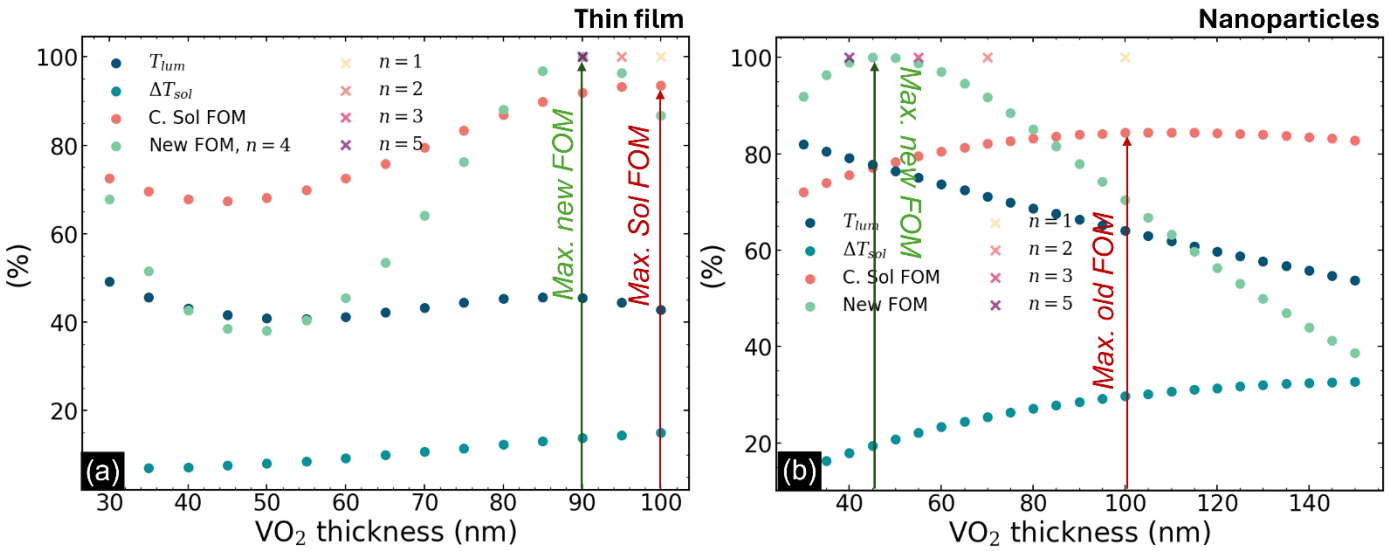

Fig. S1. Comparison between the traditional Figure of Merit (FOM) utilized in prior literature (labeled as C. Sol FOM') and the newly proposed FOM (normalized for readability) for *(a)* a VO_2 thin film and *(b)* VO_2 nanoparticles embedded in a PET matrix, both deposited on a glass substrate. The VO_2 thickness in graph *(b)* is the equivalent VO_2 thickness, *i.e.* the real thickness*0.01. In *(a)*, it is observed that the maximum value of the new FOM allows to obtain a (T_{lum}, ΔT_{sol}) pair of (45%,14%), which is to be compared to the optimized values through the old FOM, (42.5%,15%). The same observation can be made in the nanoparticles case, in graph *(b)*: The new FOM is maximimzed for T_{lum} values higher than 75% with ΔT_{sol} higher than 15%, while the old FOM is maximum for T_{lum} values that go as low as 60%, which is too low for practical applications. Furthermore, the maximum positions of the new FOM with other exponents are shown for information. It can be observed that lower values of the exponent give maxima positioned at higher VO_2 thicknesses, corresponding in each case to lower T_{lum} values. Higher values for the exponent appear to have minimal impact on the position of the maximum.

[1] Department of Physics, SPIN, University of Liège, Allée du Six Août 19, Liège B-4000, Belgium. E-mail : abaret@uliege.be
[2] Univ. Grenoble Alpes, CNRS, Grenoble INP, LMGP, Grenoble F-38016, France
[3] Univ. Bordeaux, CNRS, Bx INP, ICMCB, UMR 5026, F-33600 Pessac, France

The visualization of data points from existing literature on FOM graphs provides valuable insights. The adoption of the new FOM proves advantageous in this context, as its consistent formulation allows for a more precise and straightforward comparison between data points from different studies without the need to arbitrarily setting maximul values for the investigated parameters. Moreover, employing a standardized FOM offers several other benefits, including facilitating rapid evaluation and selection of materials for specific applications, enabling systematic optimization of device performance, and promoting interoperability and reproducibility within the scientific community. Finally, the specific shape of the determined FOM, gives more importance to results that naturally appear as better performing and suited to practical design implementation. The results of these comparisons are illustrated in Fig. S2.

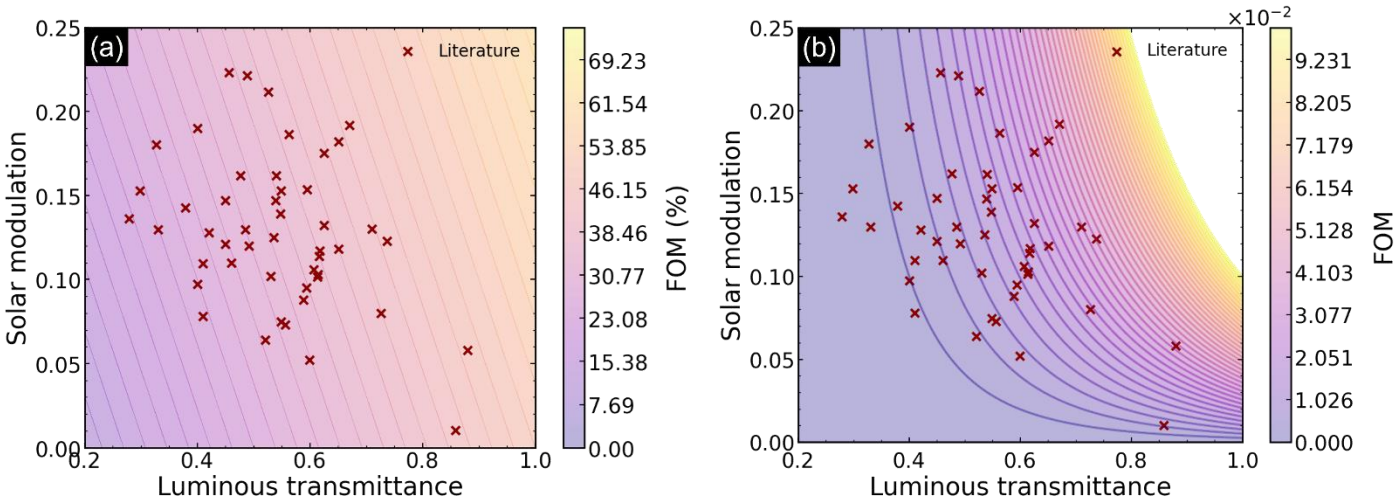

Fig. S2. FOM comparison for *(a)* the old and *(b)* the new FOM with empirical data taken from the literature. *(a)* Given the non-universality of the old FOM's shape, we opted to utilize 100% as maximum T_{lum} and ΔT_{sol} values. This normalization allows for the comparison of outcomes from various sources.

2) Additional references for refractive indices sources

In Fig. 1 of the main manuscript, we compare simulated results to empirical measurements. The details of the simulated stacks and refractive indices data references can be found in Table S1.

Stack[nm]	$\frac{T_{lum}^{sim} - T_{lum}^{exp}}{T_{lum}^{exp}}$	$\frac{\Delta T_{sol}^{sim} - \Delta T_{sol}^{exp}}{\Delta T_{sol}^{exp}}$	$\frac{FOM^{sim} - FOM^{exp}}{FOM^{sim}}$	**Refs**
SiO_2[115]/TiO_2(α)[100]/VO_2[100] /TiO_2(A) [60]/SiO_2	1%	-7%	-3%	C. Sol[1]
VO_2[80]/Cr_2O_3[40]/Glass	3%	-5%	6%	T. Chang[2]
TiO_2(A)[75]/VO_2[50]/TiO_2(A) [75]/Glass	5%	76%	111%	N.R. Mlyuka[3]
TiO_2(A)[130]/VO_2[50]/ TiO_2(A)[130]/VO_2[50]/ TiO_2(A)[130]/Glass	-15%	-19%	-59%	N.R. Mlyuka[4]
TiO_2(A)[190]/VO_2[150]/TiO_2(α) [100]/SiO_2	17%	112%	296%	J. Zheng[5]
VO_2-NPs in polymer[5000]/Glass	5%	4%	26%	S.-Y. Li[6]
Si_3N_4[50]/Ag[8]/VO_2[30]/Si_3N_4[57]/Glass	20%	67%	249%	B. Baloukas[7]
Si_3N_4[97]/Ag[8]/VO_2[30]/Si_3N_4[123]/Glass	37%	27%	346%	B. Baloukas[7]
ZnO[197]/VO_2[66]/ZnO[196]/Glass	8%	3%	38%	W. Jin[8]

VO_2[66]/ZnO[196]/Glass	24%	9%	166%	W. Jin[8]
Cr_2O_3[40]/VO_2[80]/SiO_2[30]/Glass	2%	-4%	4%	T. Chang[9]
CeO_2[180]/VO_2[30]/Glass	14%	-8%	58%	H. Koo[10]

Table S1. Results from our simulations compared to empirical measurements for various stacks identified in the literature. Many different materials were used in addition to VO_2 to extensively investigate the behavior of the simulations. Criteria for choosing a stack in a manuscript were only the determined values for the stacks layers, as well as the fact that the stacks must have been composed of only plain thin films or nanoparticles-embedded thin films. All simulations were carried assuming normal incidence. The optical properties for the VO2 layer were not changed from simulation to simulation, such that differences in this active layer properties (surface roughness, chemical stoichiometry) can lead to differences in predicted and observed measured.

Data for the refractive indices that are not listed in Table 1 of the main manuscript were identified using the Webplotdigitizer tool for the following materials, with respective references: $TiO_2(\alpha)$[1], TiO_2(A)[1], Cr_2O_3[11], Si_3N_4[12], ZnO[13], CeO_2[10].

3) Nanoparticles refractive indices and calculations

The calculations for the refractive indices associated to the PET-embedded nanoparticles were performed based on the results by Li, Granqvist (2010). Using the effective medium approach, they have shown that the effective dielectric function associated with the hybrid nanoparticles-PET matrix is given by:

$$\epsilon^{MG} = \epsilon_m \frac{1 + \frac{2}{3} f\alpha}{1 - \frac{1}{3} f\alpha},$$

Where ϵ_m is the permeability of the polymer matrix, f is the filling fraction (set to 1% in this work based on the results of Li.-Y.) and

$$\alpha = \frac{\epsilon_p - \epsilon_m}{\epsilon_m + \frac{1}{3}(\epsilon_p - \epsilon_m)}$$

With ϵ_p the permeability of the nanoparticles, which itself depends on the insulating or metallic state of the VO_2. The 0.33 factor is valid for spherical nanoparticles.

The refractive indices were then simply obtained by using the well-known relation $\tilde{n}^2 = \epsilon$, with $\tilde{n} = n + ik$.

4) Sensitivity enhancement of the VO_2/Ag interface

The mechanism behind this enhancement was unraveled by Baloukas *et al.* [7]. This increase from the Ag-less stack stems from the higher sensitivity of the VO_2/metallic interface than of the VO_2/dielectric interface to the thermochromic transition of the VO_2 layer. This can be shown more precisely by considering the Fresnel coefficients of the two layers. Fresnel's equations state that the reflectance R at the interface from layer 1 to layer 2 is given by

$$R = \left| \frac{\tilde{n}_1 - \tilde{n}_2}{\tilde{n}_1 + \tilde{n}_2} \right|^2,$$

Where $\tilde{n}_i$ is the complex refractive index of layer i. We note that in the case of absorbent layers, the imaginary part of $\tilde{n}$ cannot be neglected. In the following figure, we show the resulting graph at a VO_2/Ag or VO_2/glass interface in terms of transmittance $T = 1 - R$ (considering negligible absorption given the ultra-low thicknesses involved) and obtained solely by computing the above-mentioned formula. These results demonstrate that the difference in transmittance between the two states of the VO_2 is higher when it is on silver than when it is on glass, confirming the statement of Baloukas and explaining the reason for higher solar modulation ability reached with the silver thin film addition.

5) PET transmittance spectrum

The emissivity spectrum of the VO_2 nanoparticles-based stacks displayed in Fig. 3 of the main manuscript may appear as odd to the first view. However, this pattern is expected due to the shape of the optical properties of the PET itself under higher wavelengths illumination. Fig. S3 showcases the refractive indices and simulated transmittance spectra of simple PET in air.

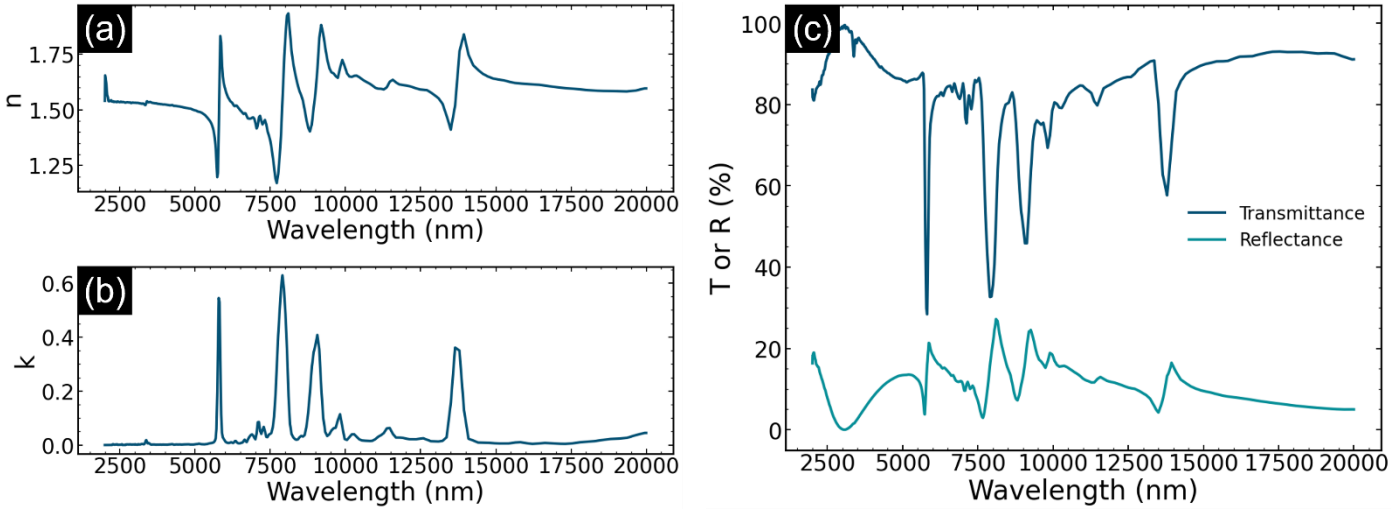

Fig. S3. Real *(a)* and complex *(b)* refractive indices of PET. *(c)* Transmittance and reflectance spectra of a plain, 1µm thick PET film. The light is coming normally to the interface.

6) Relative variation of the emissivity

Concerning the difference in emissivity reduction linked to the Ag NW network on the NP stack compared to the TF stack, one can more precisely inspect the Hanauer's semi-empirical model, which we remind here:

$$\epsilon = \sqrt{\epsilon_{Ag}^2 + \left(\epsilon_{Ag} + \epsilon_{sub}(1-\eta) + \left(\eta\epsilon_{sub} - \epsilon_{ag}\right)T_{net}\right)^2}$$

As depicted in figure *(a)* here below, this shows a linear trend between the total stack emissivity ϵ and the substrate's emissivity ϵ_{sub} for high values of ϵ_{sub}. However, as shown in figure *(b)*, for emissivities lower than 0.2, the variation of the relative variation of the stack's emissivity with that of the substrate (ϵ/ϵ_{sub}) is not linear. What is important to notice is that, as displayed in figure *(c)* below, this induces that the higher the emissivity of the substrate, the more impactful the effect of the silver nanowire network. Indeed, one can see that for very low emissivities of the substrate, the relative variation of ϵ compared to the pristine substrate becomes negligible, such that the model

itself predicts that for a stack that boasts an emissivity of 7 %, adding a silver nanowire network will have minimal impact. Alternatively, given that the NPs stack has a higher emissivity of 45 %, the nanowire network impact is not negligible and is, in fact, higher than that of the silver thin film layer.

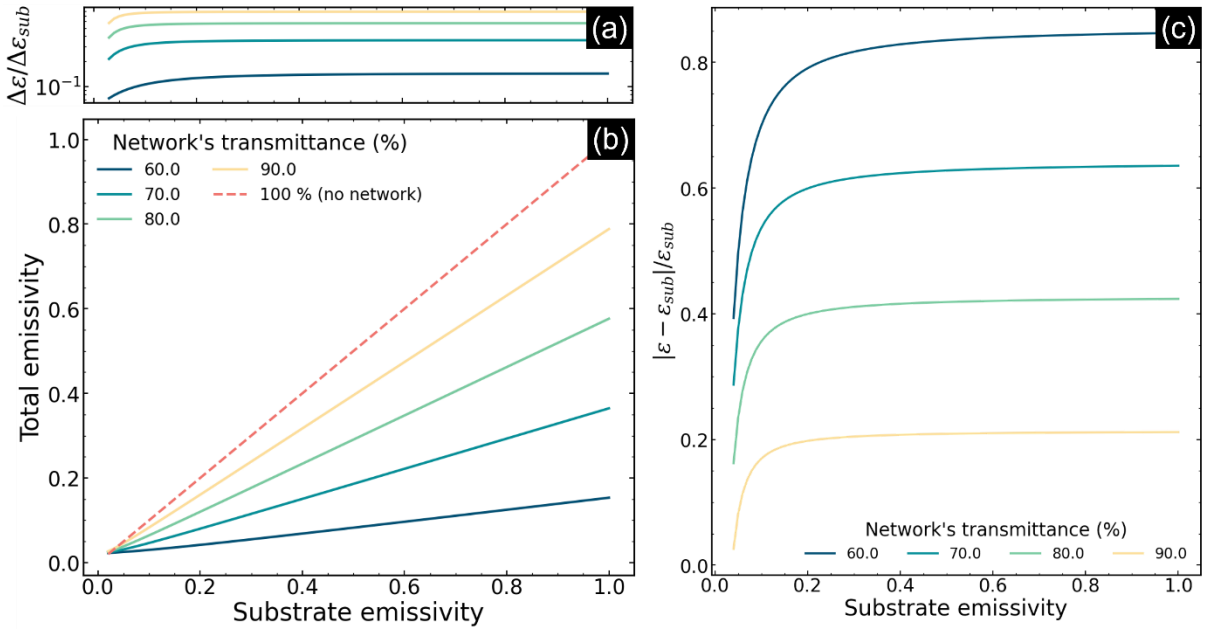

Fig. S4. Differential *(a)* and evolution *(b)* of the emissivity of a NW-coated substrate as a function of the substrate's emissivity, from Hanauer's model and for different given network's transmittances. (c) Relative variation of the emissivity with the Ag NW network coating compared to the pristine substrate's emissivity, as a function of the latter and for different network's transmittances.

References

1 C. Sol, M. Portnoi, T. Li, K. L. Gurunatha, J. Schläfer, S. Guldin, I. P. Parkin and I. Papakonstantinou, *ACS Appl. Mater. Interfaces*, 2020, **12**, 8140–8145.

2 T. Chang, X. Cao, N. Li, S. Long, X. Gao, L. R. Dedon, G. Sun, H. Luo and P. Jin, *ACS Appl. Mater. Interfaces*, 2017, **9**, 26029–26037.

3 N. R. Mlyuka, G. A. Niklasson and C. G. Granqvist, *Solar Energy Materials and Solar Cells*, 2009, **93**, 1685–1687.

4 N. R. Mlyuka, G. A. Niklasson and C. G. Granqvist, *physica status solidi (a)*, 2009, **206**, 2155–2160.

5 J. Zheng, S. Bao and P. Jin, *Nano Energy*, 2015, **11**, 136–145.

6 S.-Y. Li, G. A. Niklasson and C. G. Granqvist, *Journal of Applied Physics*, 2010, **108**, 063525.

7 B. Baloukas, S. Loquai and L. Martinu, *Solar Energy Materials and Solar Cells*, 2018, **183**, 25–33.

8 W. Jin, K. Park, J. Y. Cho, S.-H. Bae, M. Siyar, H. Jang and C. Park, *Ceramics International*, 2023, **49**, 10437–10444.

9 T.-C. Chang, X. Cao, S. Bao, S. ji, H.-J. Luo and P. Jin, *Advances in Manufacturing*, 2018, **6**, 1–19.

10 H. Koo, D. Shin, S.-H. Bae, K.-E. Ko, S.-H. Chang and C. Park, *J. of Materi Eng and Perform*, 2014, **23**, 402–407.

11 D. De Maio, C. D'Alessandro, A. Caldarelli, D. De Luca, E. Di Gennaro, R. Russo and M. Musto, *Energies*, 2021, **14**, 900.

12 K. Luke, Y. Okawachi, M. R. E. Lamont, A. L. Gaeta and M. Lipson, *Opt. Lett., OL*, 2015, **40**, 4823–4826.

13 O. Aguilar, S. de Castro, M. P. F. Godoy and M. R. S. Dias, *Opt. Mater. Express, OME*, 2019, **9**, 3638–3648.